Signal Acquisition of High-Speed Periodic Signals Using Incoherent Sub-Sampling and Back-End Signal Reconstruction Algorithms

Hyun Choi, *Student Member, IEEE,* Alfred V. Gomes, *Member, IEEE,* and Abhijit Chatterjee, *Fellow, IEEE*

***Abstract*—This paper presents a high-speed periodic signal acquisition technique using incoherent sub-sampling and back-end signal reconstruction algorithms. The signal reconstruction algorithms employ a frequency domain analysis for frequency estimation, and suppression of jitter-induced sampling noise. By switching the sampling rate of a digitizer, the analog frequency value of the sampled signal can be recovered. The proposed signal reconstruction uses incoherent sub-sampling to reduce hardware complexity. The results of simulation and hardware experiments indicate that the proposed signal reconstruction algorithms are able to reconstruct multi-tone high-speed periodic signals in the discrete time domain. The new signal acquisition technique simplifies signal acquisition hardware for testing and characterization of high-speed analog and digital signals.**

***Index Terms*—signal reconstruction, incoherent sub-sampling.**

I. Introduction

A Sampling-based signal acquisition device is frequently utilized for high-speed signal measurement and characterization. The sampling rate of such instrumentation is, however, limited in practice. To overcome such a limitation, high-speed digital oscilloscopes are equipped with equivalent-time sampling functions, which employ a fixed frequency sampling clock combined with a swept delay circuit. The digitizer captures the horizontal sweep of a periodic waveform at a relatively low sampling speed. Using timing information obtained from the swept delay circuit, the digitized samples are processed digitally to re-build the signal for a single cycle. In this sampling technique, the accuracy of the swept delay line is critical for minimizing measurement timing error. However, due to imperfections in the delay circuitry, nonlinearity and random errors are possibly introduced into the delay time; consequently, this timing error degrades the measurement accuracy. Another approach for digitizing high speed signals using low speed clocking mechanisms is the parallel sampling architecture. In this architecture, multiple samplers are used in parallel to digitize the common analog signal using independent sampling clocks that contain dedicated timing delay. In [1], the total real-time sampling rate of 20-Gsps was achieved. In the parallel sampling method, imperfections in the multiple delay lines degrade the measurement resolution in the same manner as equivalent-time sampling.

For high-speed signal spectral analysis, coherent sub-sampling is utilized [2][3]. In this approach, an analog waveform is digitized over an integer number of cycles (coherency) at a sampling speed which is lower than the Nyquist rate. Coherent sampling eliminates unwanted discontinuities in sampled signals and minimizes the spectral leakage of the signals in the frequency domain. However, the coherent sub-sampling method (for spectral analysis) has limitations. First, enabling coherency requires additional hardware for synchronizing the sampled analog signal to the sampling clock. Second, spectral content outside the sampling bandwidth is aliased, so the analog frequency information of the sub-sampled signal is lost unless the frequency of the sub-sampled signal is known precisely and the sub-sampling rate is adjusted to accommodate for that. Finally, infrequent glitches and timing noise in the signal are hard to be observed in spectrum analysis due to its averaged power measurement.

In contrast to the coherent sub-sampling based spectral measurement, a time-domain measurement using incoherent sub-sampling is presented in this paper. First, using the proposed back-end signal reconstruction algorithms, a raw incoherently sub-sampled signal is re-mapped to represent the signal within its single cycle (in the discrete time domain). Note that the proposed signal acquisition technique does not require timing circuitry such as a delay line or a synchronization module: such hardware-based timing functions are replaced by digital processing algorithms which do not require the use of additional analog hardware. From the reconstructed waveform in the discrete time domain, signal parameters such as rise/fall time, pulse width/height, signal overshoot/undershoot and ringing can be determined for test and measurement purposes (even though not evaluated in this paper). Random timing noise of the signal can be also observed in the discrete time domain. It is shown that spectral leakage related measurement inaccuracy due to incoherent sampling can be overcome using digital signal processing. In addition, by switching the sampling speed, the analog frequency value can be recovered from sampled signals. The analog frequency information of sub-sampled signals is, otherwise, lost due to spectrum aliasing distortion.

The core innovations of the signal acquisition technique proposed in this paper are:

- simplified signal acquisition architecture in terms of RF/mixed-signal designs.
- software implementation of time synchronization hardware used in traditional digital oscilloscopes.
- reduced measurement and test cost due to their ease of deployment and simplicity.

This research was supported in part by National Semiconductor Corporation and by GSRC-MARCO under Grant 2003-DT-660.

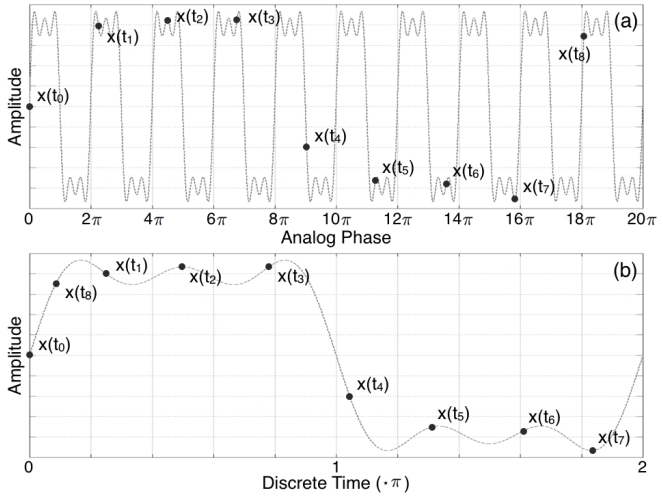

Fig. 1. Time re-mapping of an incoherently sub-sampled signal: (a) an analog periodic signal shown with its sampled data (in the raw sequence), and (b) the reconstructed waveform with the re-mapped samples in the discrete time domain.

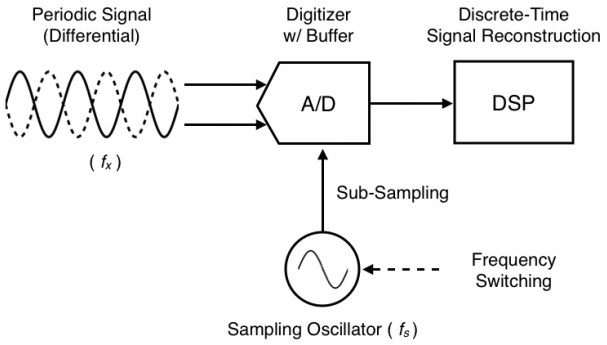

Fig. 2. The proposed incoherent sub-sampling ($f_x > f_s/2$) and signal reconstruction setup.

The remainder of the paper is organized as follows. In Section II, the proposed signal acquisition method and related theories are described. Hardware experiment results and related practical issues are summarized in Section III. Finally, conclusions are discussed.

II. Proposed Software-Based Signal Reconstruction

To prepare a sampled signal utilized by the proposed software-based signal reconstruction technique, a high-speed periodic signal, whose operation frequency is higher than half the sampling rate of the digitizer, is *incoherently sub-sampled* at a fixed rate. As shown in Figure 1-(a), the data points of the sub-sampled signal are coarsely distributed in time. Even though the time resolution of the sampled signal is not enough to completely reconstruct its real-time waveform—the Nyquist sampling criteria, the sub-sampled signal can be reconstructed in non-real-time, where the samples are re-mapped to the discrete time domain [0, 2π) as illustrated in Figure 1-(b). Each sample point contributes to re-building the waveform in the equivalent-time sense. For such signal re-mapping, standard instrumentation utilizes additional hardware such as delay and trigger signal generators. In the proposed approach, however, the signal re-mapping is enabled by the software-based signal reconstruction (described in Section II).

As shown in Figure 2, the proposed incoherent sub-sampling and signal reconstruction setup consists of an analog-to-digital converter (ADC), sampling oscillator and digital signal processor (DSP). In addition, the frequency switching function of the sampling oscillator is necessary for determining the analog frequency value of the sub-sampled signal. The ADC incoherently sub-samples a periodic analog signal in the absence of synchronization circuits, and the DSP performs frequency domain analysis to reconstruct the signal in the discrete time domain in the equivalent-time sense.

The proposed signal acquisition system operates under the following condition: (1) the frequency of the analog signal to be acquired is assumed to be unknown, and (2) the sampling oscillator contains low far-out phase noise.

A. Discrete Frequency Estimation

Discrete frequency is the frequency measure of discrete signals determined in the range of [0, π) (the term is defined in Appendix A). To reconstruct the waveform from coarsely sampled data, estimating the discrete frequency of the sampled signal is essential as described in Section II-B.

The discrete frequency value of a sampled signal can be found by locating a fundamental spectral peak of the discrete spectrum of the sampled signal. Such discrete spectral analysis, however, suffers a finite spectral resolution Δ_f, which is defined by

$$\Delta_f = \frac{\pi}{n}, \tag{1}$$

where n is the number of samples. The value of Δ_f is hardly driven small enough since the sample size n is, in practice, limited by the available memory size of a digitizer. For this reason, any discrete frequency values can be measured only at the frequency that is an integer multiple of Δ_f. Due to this reason, the discrete frequency estimation (an essential procedure in the proposed signal reconstruction method) is not accurate enough without further assistance described below.

To improve the resolution of discrete frequency estimation, *pre-* and *post-conditioning* techniques can be applied to the discrete Fourier transform (DFT) [5]. First, pre-conditioning is used to minimize the spectral leakage of the incoherently sampled signal. The incoherently sampled signal contains a discontinuity at the beginning and the end of the sample sequence. Such a discontinuity causes spectral leakage of the discrete spectrum as shown in Figure 3-(a), which results in reduced accuracy of the discrete frequency estimation. To minimize signal discontinuity and spectral leakage, the sampled signal is multiplied by a window function (windowing) and then transformed to the frequency domain using DFT. For instance, the Gaussian window, denoted by ω, can be applied to the sampled signal using the normalized Gaussian function:

$$w[k] = e^{-(k-l/2)^2/(2\sigma^2)}, \tag{2}$$

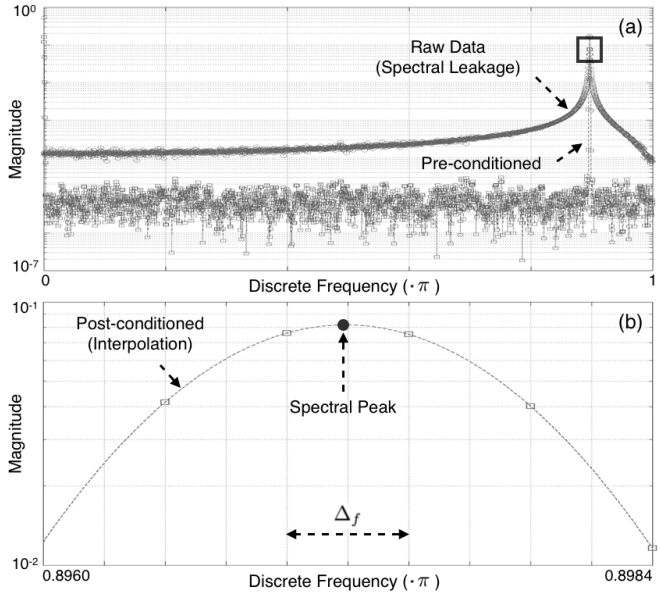

Fig. 3. Spectral analysis for sub-sampled data: (a) with and without pre-conditioning (marked as squares and circles respectively), and (b) spectral peak estimation using post-conditioning (a magnified view of the squared region in (a)).

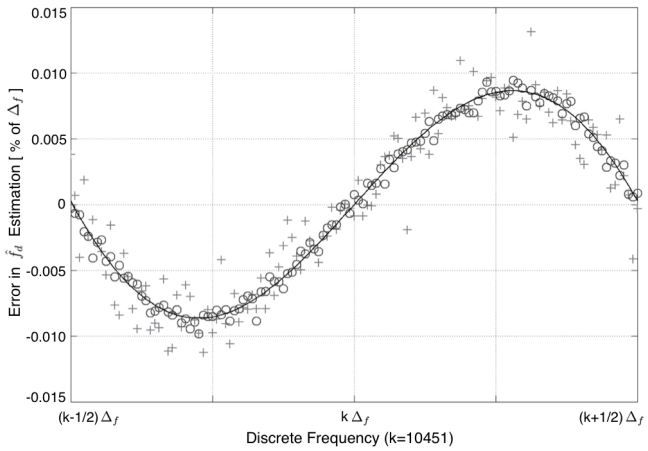

Fig. 4. Discrete frequency estimation error of digitizers with bit resolution of 10 (denoted as [+]), 12 (denoted as [o]), and a value approaching machine precision (denoted as a solid line).

where l denotes the window length, σ the standard deviation, and k=1, 2, ..., l. The formula l=n holds true when the window is applied to the entire sampled signal. It is shown in Figure 3-(a) that the spectrum obtained from the DFT with signal pre-conditioning, denoted by X, contains less spectral leakage than the unconditioned spectrum. Second, in signal post-conditioning, the spectral points are interpolated to locate the spectral peak with enhanced resolution. In Figure 3-(b), the abscissa of the spectral maximum, which falls between the spectral bins, is located by interpolating the magnitude of three frequency bins: one with the highest magnitude and its two neighbor bins. Using the Gaussian interpolation, as an example of interpolation methods, the discrete frequency estimation, $\hat{f}_d$, is calculated using the formula:

$$\hat{f}_d = \Delta_f \cdot \big(m + \frac{\ln \frac{X[m+1]}{X[m-1]}}{2 \cdot \ln \frac{X[m]^2}{X[m+1]X[m-1]}}\big), \tag{3}$$

where m denotes the index of the frequency bin with the highest magnitude.

In computer simulation, the discrete frequency estimation accuracy obtainable from the pre- and post-conditioning was evaluated. The ADC models with sampling rate of 500 Msps, 10-, 12- and 64-bit resolution, were constructed. Note that static nonlinearity was not incorporated in these models. Analog signals (sinusoids) with various frequencies were examined to determine the discrete frequency estimation accuracy at various signal frequencies: the frequency of the analog signal was swept with the center value of $k\Delta_f \approx 1.275756$ GHz (k = 10451, $\Delta_f \approx 0.1220703$ MHz), which falls exactly at the frequency bin, and with the range of $\pm\Delta_f/2$. For signal pre- and post-conditioning, a Gaussian window with $r = 8$ (the ratio between the window length n and the standard deviation) and Gaussian interpolation were used, respectively.

In Figure 4, the discrete frequency estimation errors are plotted for various swept signal frequencies. According to the plot, the amount of the estimation error depends on where the signal frequency resides between the DFT frequency bins. The simulation results of the highest resolution ADC show that the maximum estimation error is 0.0087% of Δ_f at the signal frequency of $k\Delta_f \pm 1/4\Delta_f$. As the ADC bit resolution decreases to 12 (denoted as [o]) and 10 (denoted as [+]), the estimation errors increase but are bounded by 0.015% of Δ_f.

B. Signal Reconstruction in the Time-Domain

In this section, the sampled signal x, sequenced according to raw sampling time as shown in Figure 1-(a), is re-mapped to represent the signal within a single fundamental cycle, as shown in Figure 1-(b). For signal re-mapping, the discrete frequency measure $\hat{f}_d$ obtained in Section II-A is required to determine the discrete time of the samples. Such a discrete frequency-to-time conversion (described in Appendix A in detail) can be expressed using the modulo operation. The discrete time of the k-th sample, $x[k]$, is determined in the discrete time range of [0, 2π) by

$$t_d[k] = \mathrm{mod}\big(t_d[k-1] + \hat{f}_d\ ,\ 2\pi\big), \tag{4}$$

where $\hat{f}_d$ is the estimated discrete frequency, and mod(a, b) is the modulo operation which finds the remainder of division of a by b. Note that this formula is the discrete version of the analog frequency-to-time conversion shown below.

$$\phi_x(t) = \phi_x(t - \Delta t) + \omega_x \cdot \Delta t, \tag{5}$$

where ϕ_x, ω_x, t and Δt denote the analog phase, angular frequency, time and time increment of a periodic signal, respectively. In the analog domain, the angular frequency defines the phase of a periodic signal at a particular time. In the discrete domain, on the other hand, the discrete frequency specifies the discrete time of a sampled signal at a particular sample point, as described in Equation 4. The only additional component in Equation 4 as compared to Equation 5 is the

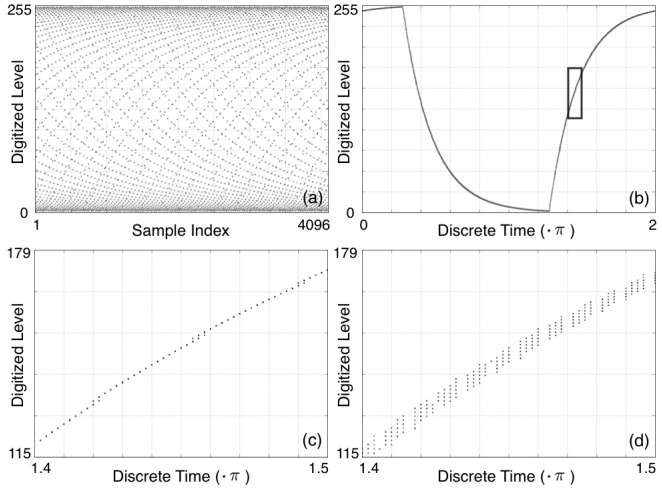

Fig. 5. Reconstruction of sub-sampled clock signal: (a) data in a raw sequence, (b) the reconstructed waveform, (c) the magnified view of the squared region in (b), and (d) the reconstructed waveform resulted from an erratic frequency estimation.

modular operation, which is required for the discrete time to be confined within the range of [0, 2π).

Due to possible estimation error in the discrete frequency measure $\hat{f}_d$ with respect to the true discrete frequency value f_d^*, the discrete time of the sampled signal can be determined incorrectly: the error in $t_d[k]$ accumulates over k (= 1, 2, ..., n). Thus, a small error ϵ_{f_d} in the estimated discrete frequency can result in large discrete time errors for large values of k

$$\epsilon_{t_d}[k] = \mathrm{mod}\big(k \cdot \epsilon_{f_d},\ 2\pi\ \big), \tag{6}$$

$$\epsilon_{f_d} = \left|\hat{f}_d - f_d^*\right|. \tag{7}$$

According to the equations above, the discrete frequency estimation error should be lower than 1% of Δ_f to bound the discrete time error to 0.01.

The proposed phase re-mapping method was simulated using a 10-bit ADC without additional amplitude and timing noise. An analog signal (square wave) was acquired at the sampling rate of 1.159 times the analog signal frequency. The discrete frequency of the sampled signal was located with an estimation error of 0.0097% of Δ_f. Using the discrete frequency measure, the sub-sampled signal was reconstructed into a single cycle of the waveform. The sub-sampled raw data and the reconstructed signal are shown in Figure 5-(a) and -(b), respectively. Figure 5-(c) is a magnified view of the squared area in Figure 5-(b). To show how the discrete frequency estimation error distorts the reconstructed signal, the error of 1% of Δ_f was intentionally applied to $\hat{f}_d$. The waveform reconstructed from the erratic frequency measure is plotted in Figure 5-(d), which shows discrete time dispersion of $\approx 0.01\pi$ (peak-to-peak value).

C. Jitter-Induced Noise Suppression

In case a sampling oscillator is unstable and generates a signal with timing noise (or jitter), the sampled signal obtained from this unstable time-base contains jitter-induced sampling noise. The waveform that is reconstructed from such a noisy sampled signal also involves discrete time noise in the discrete time domain. This type of noise in the reconstructed waveform is represented as a time-dispersed waveform in the discrete time domain.

To compensate the reconstructed waveform for jitter-induced sampling noise, a discrete frequency tracking method is used. Timing jitter of an unstable oscillator can be seen as unstable (or time-varying) operation frequency in the frequency domain. For this reason, the time-varying frequency information of the sampling oscillator is used for jitter tracking (or compensation), instead of using the constant (or averaged) frequency value as shown in Equation 4. In addition, the time-varying frequency information does not need to be measured directly from the sampling oscillator, rather observed indirectly from time-varying components in the discrete spectrum of the sampled signal. Note that the time-varying (discrete) frequency tracking method only suppresses long-term jitter components since it does not track short-term fluctuations in sampling frequency.

Time-varying discrete frequency can be detected by using the short-time Fourier transform (STFT) of the sampled signal, where each of the time-windowed signal spectrum represents the frequency components within the time period of the time-windowed signal. The estimated discrete frequency value (from the STFT results) as a function of the sample index k, $\hat{f}_d[k]$, is used for the discrete frequency-to-time conversion (the modification of Equation 4):

$$t_d[k] = \mathrm{mod}\big(t_d[k-1] + \hat{f}_d[k]\ ,\ 2\pi\big). \tag{8}$$

Since $\hat{f}_d[k]$ tracks the frequency fluctuation of the sampling oscillator over time, Equation 8 results in the discrete time value of $t_d[k]$ that compensates for jitter of the unstable sampling oscillator. Thus, the reconstructed signal based on $t_d[k]$ contains less dispersion in the discrete time domain. In fact, the jitter compensation bandwidth is determined by the discrete frequency detection bandwidth of the STFT-based spectral analysis.

The proposed noise suppression technique was evaluated using computer simulation. A harmonically related multi-tone signal (the fundament of ≈3.853 GHz and its third and fifth order harmonics) were generated and digitized (assuming no quantization errors). First, the sampled signal was reconstructed into the [0, 2π) discrete time range with and without the jitter-induced noise suppression. The performance of the noise suppression was evaluated by comparing the noise-suppressed result to the one without noise-suppression. On the merit of simulation, the discrete time dispersion of the reconstructed waveforms can be quantized directly from the plot of the sample index versus phase (time) error as shown in Figure 6. The phase noise applied to the 1 GHz sampling oscillator is denoted by (a). The phase estimation (b) is based on Equation 4 (the constant discrete frequency estimation), and the phase estimation (c) is from Equation 8 (the time-varying discrete frequency estimation). The time-varying discrete frequency value used to generate the plot (c) is derived by using the time window width of 1024 samples and shown in Figure 7. The reconstructed waveforms based on (b)

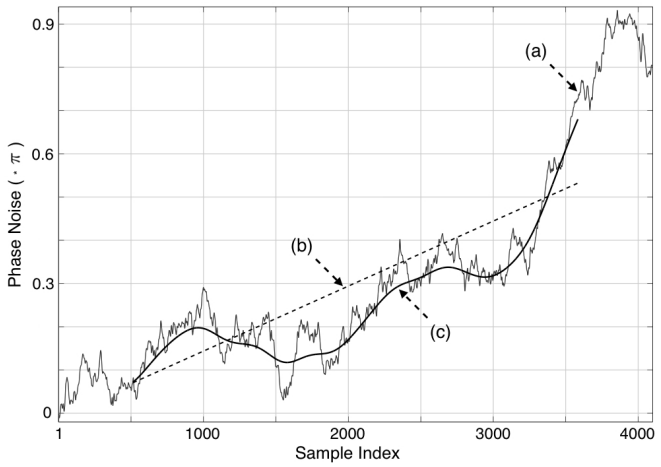

Fig. 6. Phase noise estimation: (a) the instantaneous phase noise of a sampling oscillator, (b) the phase noise estimation based on the constant discrete frequency measure, and (c) the phase noise estimation using the STFT-based time-varying discrete frequency detection.

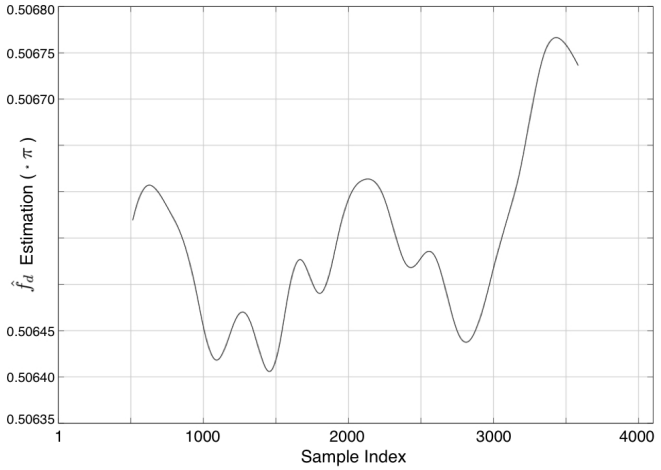

Fig. 7. STFT-based time-varying discrete frequency estimation.

and (c) are shown in Figure 8(a) and Figure 8(b) respectively. The amounts of discrete time dispersion in the two waveforms were calculated from the data in Figure 6. The reconstructed signal without the noise suppression in Figure 8(a) contains the discrete time dispersion of ≈0.12067 rms, and the one with the noise suppression in Figure 8(b) contains the discrete time dispersion of ≈0.027786 rms.

D. Analog Frequency Recovery

Conventional sub-sampling architectures are not able to extract analog frequency information from digitized signals because of spectrum aliasing distortion. Only the discrete frequency is retained in discrete signals. On the contrary, to enable a digitizer to specify the analog frequency of sampled signals, the proposed technique utilizes a sampling rate switch. As the sampling speed deviates by a small amount (digitally controlled in hardware), the analog frequency of the sampled signal can be located by observing the vector of discrete line spectra movement. In the case that analog frequency value f_x

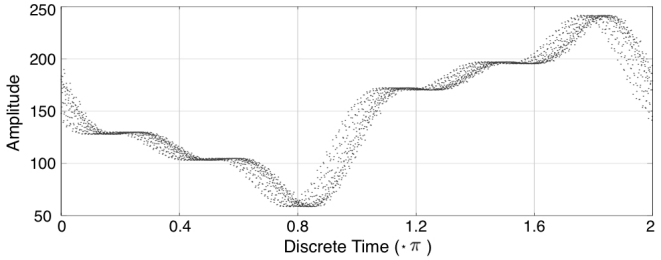

(a) A simulation result of the reconstruction of a multi-tone signal without jitter-induced noise suppression.

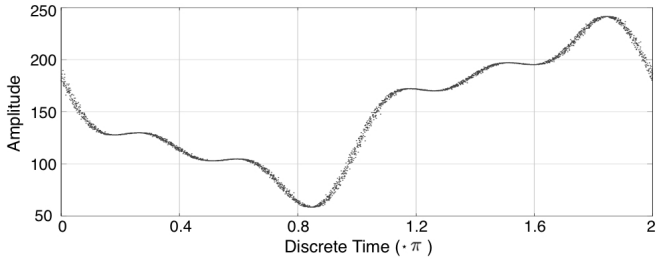

(b) A phase-noise suppressed form of Figure 8(a) using the time-varying discrete frequency estimation and jitter-induced noise suppression technique.

Fig. 8. Comparison of the signal reconstruction with and without jitter-induced noise suppression.

resides in the k-th Nyquist range

$$(k-1)\cdot\frac{f_s}{2} < f_x < k\cdot\frac{f_s}{2}, \tag{9}$$

where k is a positive integer and f_s is the sampling frequency, the spectral peak in the discrete spectrum is located at

$$\hat{f}_d = |f_x - \lfloor\frac{k}{2}\rfloor f_s|\cdot\frac{\pi}{f_s/2}, \tag{10}$$

by definition of discrete frequency described in Appendix A. The absolute value operator, $|f_x - \lfloor\frac{k}{2}\rfloor f_s|$, is introduced to address a folding effect which occurs when a sampled signal is aliased in the discrete frequency domain, and the term, $\frac{\pi}{f_s/2}$, is a normalization factor for the discrete frequency range [0, π). If the sampling speed of the digitizer is switched from f_s to $f_s + \Delta f_s$, the spectral peak is re-located to

$$\hat{f}_d + \Delta\hat{f}_d = |f_x - \lfloor\frac{k}{2}\rfloor(f_s+\Delta f_s)|\cdot\frac{\pi}{(f_s+\Delta f_s)/2}. \tag{11}$$

Subtracting Equation 10 from Equation 11, the amount of discrete frequency shift is determined as

$$\Delta\hat{f}_d = \begin{cases} -f_x\cdot\frac{2\Delta f_s}{f_s(f_s+\Delta f_s)}\cdot\pi & k=\text{odd} \\ +f_x\cdot\frac{2\Delta f_s}{f_s(f_s+\Delta f_s)}\cdot\pi & k=\text{even} \end{cases}. \tag{12}$$

Solving for f_x using Equation 12, the analog frequency value f_x is *preliminarily* determined as,

$$f_x = |\frac{\Delta\hat{f}_d}{\pi}|\cdot\frac{f_s(f_s+\Delta f_s)}{2\Delta f_s}. \tag{13}$$

Note that $\Delta\hat{f}_d$ and Δf_s are possibly incorrect due to limited measurement accuracies. The analog frequency value f_x obtained in Equation 13 is used only for determining the Nyquist range index k. Resolving for f_x using Equation 10, f_x is

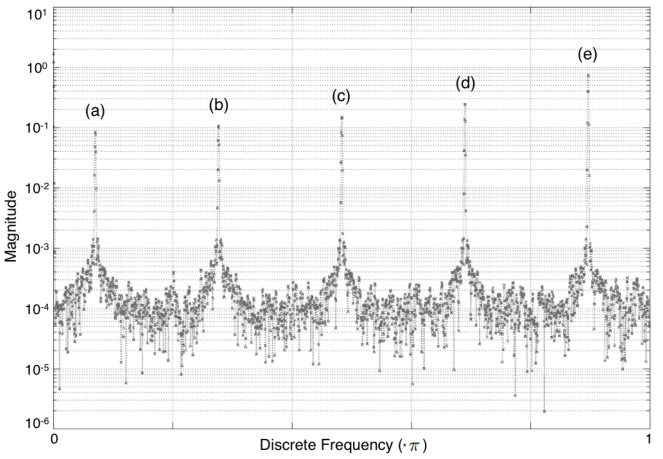

Fig. 9. The spectra of the multi-tone periodic signal (sub-sampled at 500 Msps).

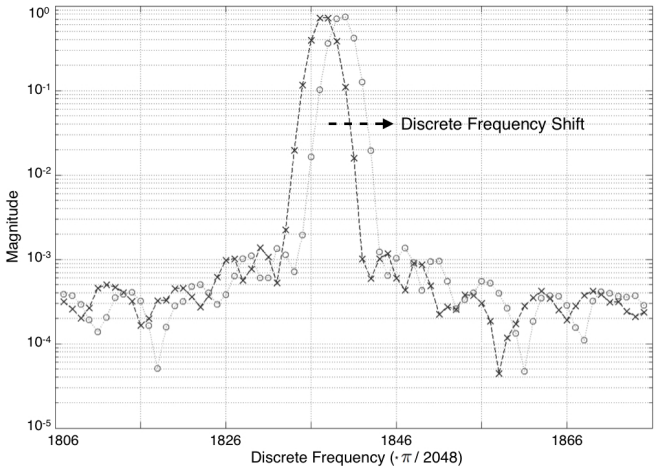

Fig. 10. The sampling speed switching differentiates the discrete frequency of the sampled signal-(e): (x) at sampling speed of 500 Msps, and (o) at sampling speed of 500.1 Msps.

determined using k, the Nyquist range index determined using Equation 9.

$$f_x = \begin{cases} \lfloor \frac{k}{2} \rfloor f_s + \frac{\hat{f}_d \cdot f_s}{2\pi} & k = \text{odd} \\ \lfloor \frac{k}{2} \rfloor f_s - \frac{\hat{f}_d \cdot f_s}{2\pi} & k = \text{even} \end{cases}, \tag{14}$$

assuming the sampling frequency f_s is known accurately.

The amount of the discrete frequency shift, $\Delta\hat{f}_d$, due to the digitizer sampling frequency switching is, in general, smaller than DFT frequency resolution. However, the value of $\Delta\hat{f}_d$ is still resolvable if signal pre- and post-conditioning described in Section II-A are used to enhance DFT resolution. To determine the feasibility of the analog frequency recovery, a computer simulation was performed. In the simulation, a noisy multi-tone signal (≈1.276-GHz square wave which consists of up to the ninth harmonic of the fundamental tone, which shows an SNR of 95.91 dB) was incoherently sub-sampled at the sampling speed of 500 Msps. In Figure 9, the spectra of the multi-tone signal (before applying the sampling frequency switching) are shown. First, the analog frequency cannot be extracted due to spectrum aliasing. Second, the fundamental tone, which is noted as (e) in Figure 9, can be identified only under the assumption that the fundamental frequency contains the highest power. To resolve these limitations, the same multi-tone signal was re-sampled at the sampling speed of 500.1 Msps. Then, spectral locations of two sampling results are compared to each other for specifying $\Delta\hat{f}_d$. The discrete frequency shift of the spectrum (e) due to the sampling frequency switching is shown in Figure 10. The obtained simulation results are summarized in Table I: The spectrum (e) represents the fundamental tone (1.276 GHz) of the sampled multi-tone signal, and the spectra (d), (c), (b) and (a) are the 3rd, 5th, 7th and 9th harmonics respectively.

TABLE I
SAMPLING FREQUENCY SWITCHING RESULTS

Tone	Δf_s (kHz)	$\hat{f}_d$ $(\cdot\pi)$	$\Delta\hat{f}_d$ $(\cdot\pi)$	k	f_x (GHz)
(a)	100	0.070992	0.009183	46	11.482
(b)	100	0.277546	0.007143	36	8.931
(c)	100	0.484101	0.005101	26	6.379
(d)	100	0.690656	0.003061	16	3.828
(e)	100	0.897211	0.001020	6	1.276

E. Problematic Sample Distribution

In some problematic sampling cases, a reconstructed signal contains samples that are stuck together in the discrete time domain. Under such conditions, the discrete time values of multiple samples are identical, and those samples locate at the same position in discrete time. Consider, for instance, a coherent sub-sampling case in which two entire cycles of a periodic signal are sampled at eight points in time. The discrete time values of the samples are consecutively 0, $(1/2)\pi$, π, $(3/2)\pi$, 0, $(1/2)\pi$, π, $(3/2)\pi$. The first four samples form one cycle of the signal, and the other four samples construct another cycle of the signal, which is identical to the previous one. Some samples are stuck to the others, and the information contents of the samples are duplicated. For this reason, the effective sampling rate is reduced to twice the Nyquist rate. To prevent this, the number of cycles of the signal to be sampled can be changed (three cycles of the signal are sampled at eight points in time). The resulting samples are not stuck (or close) to each other. Such a solution to problematic coherent sampling is generalized and shown in Appendix B. In contrast, perfect duplication of sample contents may not occur in incoherent sub-sampling, but the effective sampling rate can be compromised for a similar reason. Consider an incoherent sub-sampling case in which 2.01 cycles of a periodic signal are sampled at eight points in time. This incoherent sub-sampling case is very similar to the previous problematic coherent sub-sampling case. The samples are not perfectly stuck together, but located very close to each other. Since the samples are not equally distributed over the signal, the effective sampling rate of the digitizer is compromised. As a solution to this problematic incoherent sub-sampling case, the sampling speed can be adjusted and the number of cycles to be sampled is different from that of any problematic coherent sub-sampling cases. See Appendix B for a generalized formulation.

A reconstructed signal with stuck samples is shown in

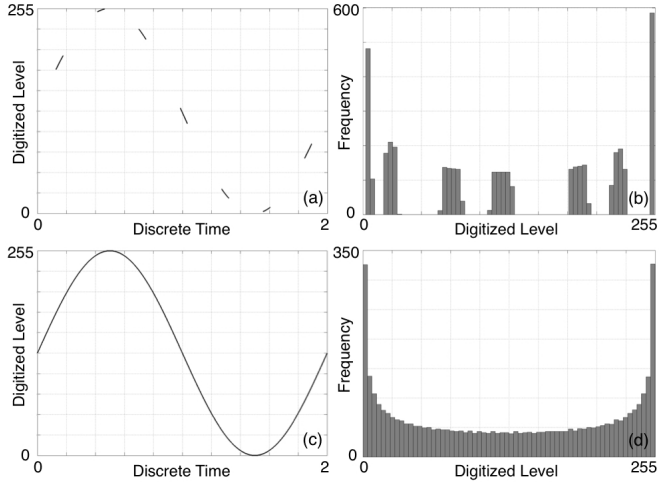

Fig. 11. Distribution of the digitized samples: (a) a localized reconstructed signal, (b) the histogram obtained from (a), (c) an unlocked reconstructed signal, and (d) the histogram obtained from (c)

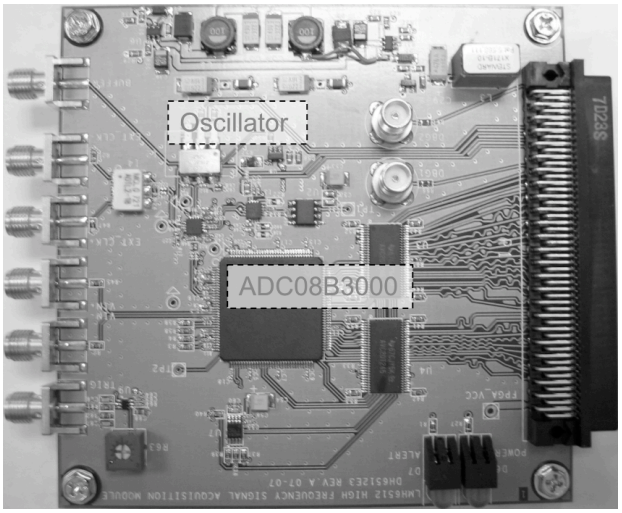

Fig. 12. Picture of the incoherent sub-sampling digitizer with the interface to an FPGA.

Figure 11(a) using computer simulation. The corresponding sample distribution contains null bins as shown in Figure 11(b). To release the stuck samples, a small offset frequency was injected to the sampling frequency, and the analog signal was re-sampled. The re-sampled signal is distributed over the entire dynamic range of the signal as shown in Figure 11(c) and shows an unlocalized distribution as shown in Figure 11(d). Note that, in hardware experiments, the sampling frequency control is enabled by a frequency controllable sampling oscillator (a voltage-controlled surface acoustic wave (SAW) oscillator with a digital frequency control is used in Section III).

III. Hardware Experiment

The proposed incoherent sub-sampling architecture was implemented on a printed circuit board (PCB) utilizing a digitizer (National Semiconductor ADC08B3000) with 8-bit resolution, 3-GHz bandwidth, 4-kByte built-in memory as shown in Figure 12. The sampling clock for the digitizer was provided by a surface acoustic wave (SAW) based voltage controlled oscillator (Crystek CVS575) whose nominal frequency is 719 MHz. This oscillator is equipped with a digital control to its operation frequency. In addition, the signal reconstruction was performed using a field programable gate array (FPGA) (XC3S200 Spartan3) on a separate PCB.

A. Discrete Frequency Estimation

When the discrete frequency estimation is evaluated in hardware, it may be less accurate than that in software simulation due to hardware non-idealities. In this subsection, first, the accuracy of the discrete frequency measurement, which is described in Section II-A, is verified in hardware. Second, a fine tuning of the obtained discrete frequency value f_d is performed to obtain a more accurate value of f_d. In this fine tuning, the discrete frequency deviation (up to 1% of Δ_f) is added the initially estimated value of f_d, and the deviated frequency value is re-applied to the discrete frequency-to-time conversion shown in Equation 4. The sampled signal is iteratively reconstructed based on each deviated value of f_d. Based on the iterative method, the value of more accurate measures of f_d can be obtained by searching for the best reconstructed signal (the least discrete time dispersion).

For experimental purpose, a 1.5-GHz sinusoidal waveform was generated from a signal generator (Agilent E4437B), and fed to the signal acquisition board. The discrete frequency of the sampled signal was calculated in the FPGA using the pre- and post-conditioning technique described in Section II-A, and denoted as $\hat{f}_d$ in Figure 13. To evaluate frequency measurement accuracy, the discrete time dispersion of the reconstructed signal (based on $\hat{f}_d$) was computed and denoted by the label *DFT-based* in Figure 13. The deviation of up to $\pm 1\%$ of Δ_f is applied to the initially obtained discrete frequency $\hat{f}_d$, and the sampled signal is iteratively reconstructed. The discrete time variance values of each reconstructed signal are plotted. The lowest discrete time variance (phase dispersion) assumably corresponds to the exact measure of the discrete frequency. The estimated discrete frequency value after the fine tuning (denoted by the label *variance-based*) shows the estimation error of $\approx$(-)0.2% of Δ_f in this particular experimental setup.

B. Jitter-Induced Noise Suppression

To evaluate the performance of the jitter-induced noise suppression technique described in Section II-C, a 1-GHz digital clock signal generated by an Agilent 8133A signal generator is incoherently sub-sampled. In Figure 14(a), the reconstructed signal based on the constant discrete frequency measure is shown. Any dispersion of the reconstructed signal in the discrete time domain is due to sampling time errors, assuming the sampled analog signal is clean. Using the time-varying discrete frequency measure, the signal reconstruction was revised as shown in Figure 14(b). This noise-suppressed reconstructed waveform contains less phase spread compared to the waveform in Figure 14(a). To quantize the amounts of phase dispersion of the waveforms in Figure 14(a) and 14(b), a virtual clean reference waveform is necessary. Such a reference

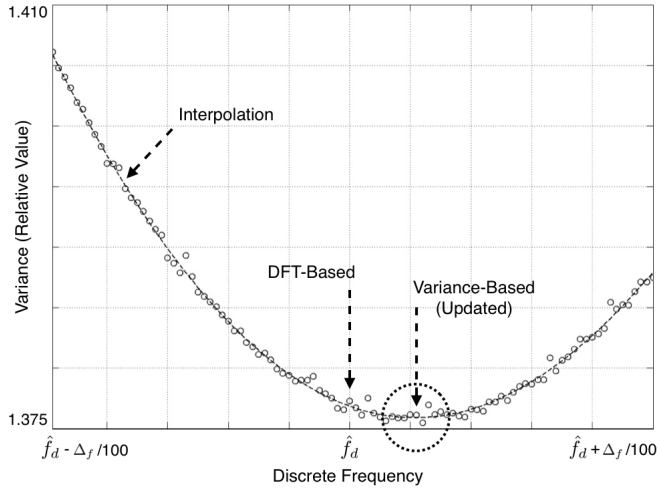

Fig. 13. Discrete frequency estimation by searching for the reconstructed signal with the least time variance.

waveform was obtained by regressing the waveform in Figure 14(b). Comparing to the obtained reference waveform, the discrete time dispersion of the two waveforms was calculated. In Figure 14(c), the dispersion of the waveform in Figure 14(a) is shown in the histogram (a) showing the standard deviation of ≈0.0031472, and Figure 14(d) calculated from the waveform in Figure 14(b) represents the standard deviation of ≈0.0014099.

C. Comparison with Standard Instrumentation

To compare the proposed signal acquisition technique with the other standard instruments, a high-frequency analog signal (pulse) was digitized using both the proposed signal acquisition board and a commercial digital oscilloscope (WavePro 7000A, 20-Gsps effective sampling rate, 3-GHz bandwidth) using the experimental setup shown in Figure 15. Through the path (a) noted in the figure, differential analog signals were digitized (sub-sampled) by the signal acquisition board, and the discrete frequency estimation and signal reconstruction were performed in the following FPGA and computers. To recover the analog frequency of the digitized signals, the sampling speed was switched to a slightly different frequency ($\Delta f_s \approx 1.305$ MHz) using the digital control implemented on the FPGA board.

The results of sampling 1-GHz, 2-GHz and 3-GHz pulse signals are plotted in Figure 16, where (a), (c) and (e) are the results acquired from the WavePro 7000A, and (b), (d) and (f) are from the proposed method. Notice that displayed waveforms from the WavePro 7000A are the averaged values, which do not represent a dispersion due to sampling time inaccuracy. In comparison, the waveforms obtained from the proposed method contain 4096 samples without averaging. In addition, the calculated rise/fall time, peak-to-peak voltage and slew rate are summarized in Table II.

D. Clock Jitter Requirement

A high-speed ADC demands a low-jitter sampling clock to preserve signal-to-noise ratio (SNR). In particular, the best

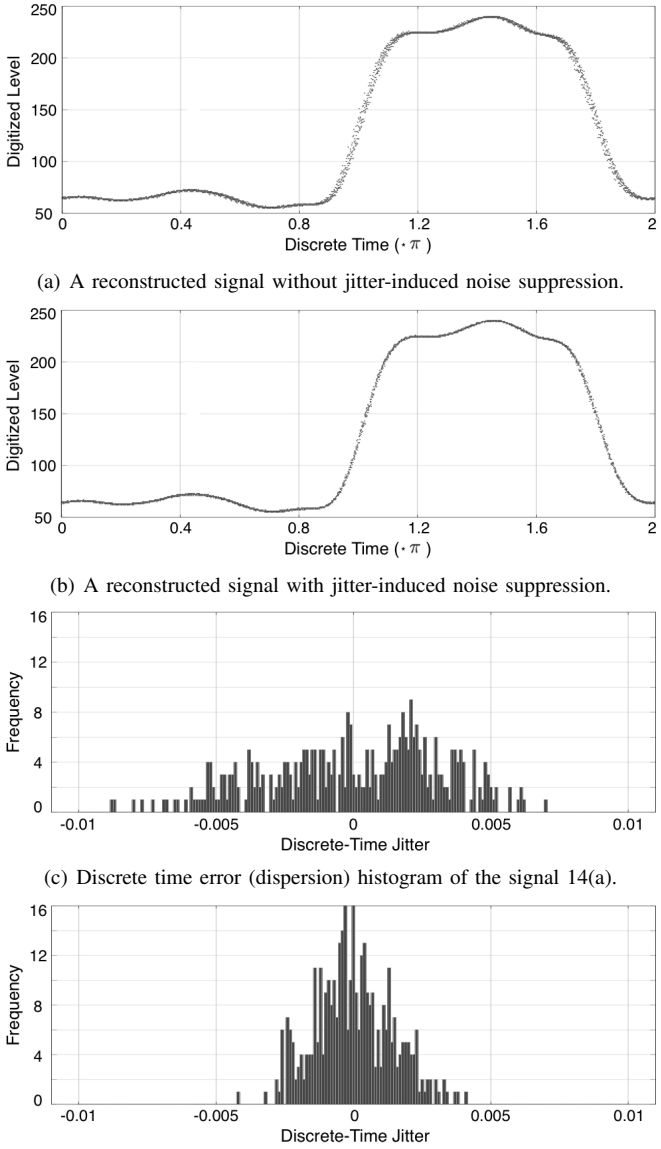

(a) A reconstructed signal without jitter-induced noise suppression.

(b) A reconstructed signal with jitter-induced noise suppression.

(c) Discrete time error (dispersion) histogram of the signal 14(a).

(d) Discrete time error (dispersion) histogram of the signal 14(b).

Fig. 14. Hardware experiment of jitter-induced noise suppression.

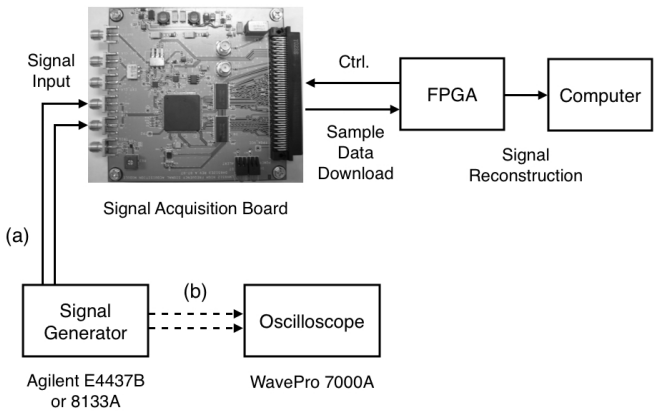

Fig. 15. A hardware experiment setup for signal acquisition using both (a) the DSP-based incoherent undersampling technique and (b) a commercial digital oscilloscope.

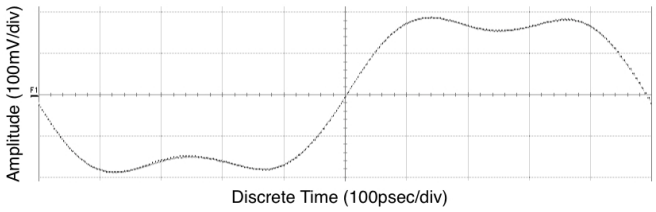

(a) A 1-GHz reconstructed clock signal obtained from WavePro 7000A (averaging mode).

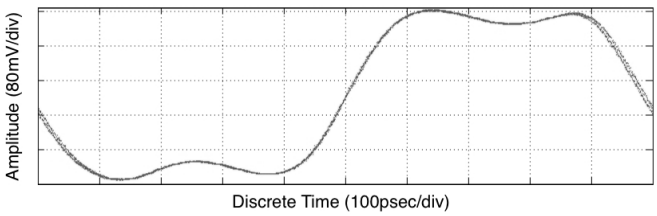

(b) A 1-GHz reconstructed clock signal obtained from the proposed method.

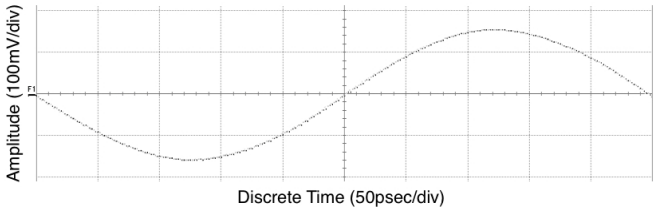

(c) A 2-GHz reconstructed clock signal obtained from WavePro 7000A (averaging mode).

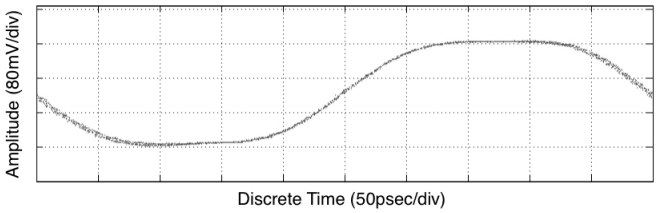

(d) A 2-GHz reconstructed clock signal obtained from the proposed method.

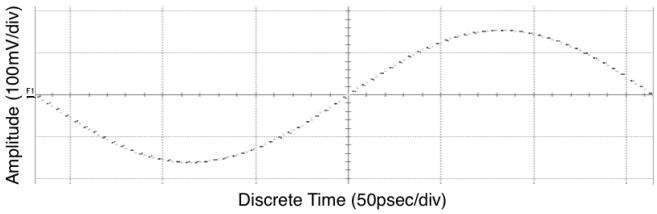

(e) A 3-GHz reconstructed clock signal obtained from WavePro 7000A (averaging mode).

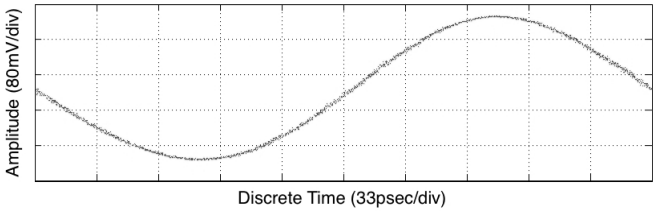

(f) A 3-GHz reconstructed clock signal obtained from the proposed method.

Fig. 16. Comparison with the standard instrumentation and the proposed signal acquisition.

TABLE II
SIGNAL MEASUREMENT FROM DIGITIZED SAMPLES IN FIGURE 16

Case	Risetime (ps)	Falltime (ps)	Pk-Pk (mV)	Slew Rate (V/ns)
(a)	135	129	376	2.228
(b)	145	148	403	2.333
(c)	120	125	316	2.207
(d)	95	102	250	2.305
(e)	101	100	319	2.527
(f)	94	105	333	2.834

case noise floor of the digitizer (National Semiconductor ADC08B3000), which is used for the hardware experiment in Section III, is -49.9 dBc/Hz. From this level, the noise floor increases further due to noise factors such as sampling clock jitter, intrinsic ADC aperture jitter, ADC nonlinearity, and thermal noise voltage. If only aperture jitter and sampling clock jitter are considered (assuming the other noise factors are negligible), total SNR can be derived from these jitter values and the analog signal frequency f_x [13]. According to manufacturer datasheets for the digitizer and the sampling oscillator (Crystek CVS575), which are used for the hardware experiment, the aperture jitter and the sampling clock jitter are specified as 400 fs rms and 200 fs rms (max, 0.05-80 MHz) respectively. The achievable total SNR is calculated for various frequencies of the analog signal to be sampled as shown in Table III.

TABLE III
ACHIEVABLE SNR (FOR VARIOUS ANALOG FREQUENCY f_x)

f_x (GHz)	SNR (dB)	f_x (GHz)	SNR (dB)
0.5	49.1	3.0	40.9
1.0	47.4	3.4	39.7
1.5	45.5	4.0	38.6
2.0	43.8	4.5	37.7
2.5	42.2	5.0	36.8

In addition, the far-out jitter (phase noise) of the sampling clock oscillator is critical because the signal acquisition time of the proposed technique is relatively short; it takes 2.848 μs to collect 4096 samples for 1.438 Gsps sampling speed. The incorporated sampling oscillator presents phase noise of -138.11 dBc/Hz and -137.72 dBc/Hz at the offset of 100 kHz and 1 MHz, respectively.

IV. CONCLUSION

A high-speed signal acquisition and software-based signal reconstruction techniques are presented in this paper. In the FPGA, an incoherently sub-sampled signal is reconstructed to form a single cycle of the waveform. The analog frequency of the sampled signal is recovered using sampling speed switch, which is incorporated in the sampling oscillator. According to experimental results, the proposed signal acquisition and reconstruction technique is able to obtain precise reconstructed waveforms.

APPENDIX A
DISCRETE FREQUENCY AND TIME

A brief overview of discrete frequency and time is described in this appendix. The definitions of discrete frequency (in case

of spectral aliasing) and discrete time are given as follows.

Definition 1: Discrete frequency f_d, as the analogue for discrete signals as analog frequency f_x is to continuous signals, is determined as

$$f_d = \frac{\min(|f_x - n \cdot f_s|)}{f_s} \cdot 2\pi, \tag{15}$$

where n is an integer, the function $\min()$ returns the smallest value of the input augments with various n, f_s is the sampling frequency, and the discrete frequency value f_d is in the range of [0, π). The function $\min(|f_x - n \cdot f_s|)$ models spectral aliasing due to undersampling, and $\frac{2\pi}{f_s}$ normalizes the discrete frequency to π.

Definition 2: Discrete time of a sampled signal is determined as

$$t_d[k] = \mathrm{mod}(k \cdot f_d,\ 2\pi), \tag{16}$$

where k is the index of the sampled signal, f_d is the discrete frequency of the sampled signal, the function $\mathrm{mod}(x,\ y)$ returns $(x - n \cdot y)$ and n is the greatest integer less than or equal to x/y, and the discrete time value $t_d[\cdot]$ is in the range of [0, 2π). Equation 16 is expanded and equivalent to Equation 4 shown in Section II-B.

$$\begin{aligned} t_d[k] &= \mathrm{mod}\big((k-1) \cdot f_d + f_d,\ 2\pi\big) \\ &= \mathrm{mod}\big(\mathrm{mod}((k-1) \cdot f_d,\ 2\pi) + f_d,\ 2\pi\big) \\ &= \mathrm{mod}\big(t_d[k-1] + f_d,\ 2\pi\big). \end{aligned} \tag{17}$$

Note that the hat symbol attached to f_d in Equation 4 indicates an estimated value.

APPENDIX B
PROBLEMATIC SAMPLING COHERENCE

Incoherent sampling can be almost coherent even though not intended depending on the sampled signal frequency. Some of coherent sampling is problematic where multiple samples of a reconstructed waveform contain the same (or similar) discrete time value, which is called stuck samples in this paper. When such sampling coherency occurs and how to escape from the coherency are described in this appendix. First, coherent sampling is defined as follows.

Definition 3: Coherent sampling is the sampling of a periodic signal, where the sampled signal represents an integer number of its cycles within the sampled set.

$$\frac{f_d}{2\pi} = \frac{n_c}{n_s}, \tag{18}$$

where f_d denotes the (fundamental) discrete frequency of the sampled signal, n_c the integer number of cycles, and n_s the number of samples.

When the rational number n_c/n_s in Equation 18 is reducible, multiple samples of the sampled signal are stuck together in the reconstructed waveform in the discrete time domain [0, 2π). As the result of such special cases of coherent sampling, gaps among samples in the discrete time domain may be too wide. Assuming that the gap larger than $2/(2^\alpha\pi)$ is unacceptable, the sampling at the following frequency bands is considered problematic in terms of sample distribution.

$$\frac{k}{2^{\alpha-1}\pi} - \Delta f_e < f_d < \frac{k}{2^{\alpha-1}\pi} + \Delta f_e, \tag{19}$$

$$\begin{aligned} \Delta f_e &= \big(\frac{2}{2^{\alpha-1}\pi} - \frac{2}{2^\alpha\pi}\big)/(n_s - 2^{\alpha-1}) \\ &= \frac{2}{2^\alpha(n_s - 2^{\alpha-1})\pi}, \end{aligned}$$

where f_d denotes the discrete frequency of the sampled signal, Δf_e the escape frequency, n_s the number of samples, and k = 0, 1, ..., α-1, α. The equispaced frequency values $k/(2^{\alpha-1}\pi)$ in Equation 19 correspond to the cases of stuck samples (the sampling coherence with the reducible rational number n_c/n_s). By moving the sampling frequency apart from such frequency values, stuck samples start to separate. The scape frequency Δf_e is the amount of the frequency movement required to separate the samples and force the discrete time gaps less than or equal to $2/(2^\alpha\pi)$.

ACKNOWLEDGMENT

The authors would like to thank the amplifier test development group members at National Semiconductor Corp. for their support on the project.

REFERENCES

[1] Ken Poulton, Robert Neff, Brian Setterberg, Bernd Wuppermann, Tom Kopley, Robert Jewett, Jorge Pernillo, Charles Tan, and Allen Montijo, "A 20GS/s 8b ADC with a 1MB Memory in 0.18μm CMOS," ISSCC Digest of Technical Papers, vol. 1, pp. 318-496, Feb. 2003.

[2] R. J. Fink, M. B.Yeary, M. Burns, and D. W. Guidry, "A DSP-Based Technique for High-Speed A/D Conversion to Generate Coherently Sampled Sequences," IEEE Trans. on Instrumentation and Measurement, vol. 52, pp. 950-958, June 2003.

[3] M. Burns, "Coherent Undersampling Digitizer for Use with Automatic Field Test Equipment," U.S. Patent, 5 589 763, 1995.

[4] A. Hajimiri and T. H. Lee, "A General Theory of Phase Noise in Electrical Oscillators," IEEE J. Solid-State Circuits, vol. 33, pp. 179-194, Feb. 1998.

[5] M. Gasior and J. L. Gonzalez, "Improving FFT Frequency Measurement Resolution by Parabolic and Gaussian Spectrum Interpolation," Beam Instrument Workshop, vol. 732, pp. 276-285, Nov. 2004.

[6] E. Mobilon, M. R. X. Barros, and A. Lopes, "Experimental verification of an eye diagram reconstruction technique based on asynchronous undersampling," Microwave and Optoelectronics Conf., pp. 603-606, July 2005.

[7] J. Redd and C. Lyon, "Spectral content of NRZ test patterns," EDN magazine, Sep. 2004.

[8] A. Parssinen, R. Magoon, S. I. Long, and V. Porra, "A 2-GHz subharmonic sampler for signal downconversion," IEEE Trans. on Microwave Theory and Techniques, vol. 45, no. 12, Dec. 1997.

[9] Y.-C. Jenq, "Perfect reconstruction of digital spectrum from nonuniformly sampled signals," IEEE Trans. on Instrumentation and Measurement, vol. 46, no. 3, pp. 649-652, June 1997.

[10] B. Razavi, "A study of phase noise in CMOS oscillators," IEEE J. of Solid-State Circuits, vol. 31, no. 3, pp. 331-343, Mar. 1996.

[11] Y. Langard, J.-L. Balat, J. Durand, "An improved method of ADC jitter measurement," International Test Conference, pp. 763-770, Oct. 1994.

[12] J. Phillips and K. Kundert, "Noise in mixers, oscillators, samplers, and logic: an introduction to cyclostationary noise," The Designer's Guide Community, 2006.

[13] J. Catt, "Clocking high-speed A/D converters," National Semiconductor Application Note, 2007.

[14] S. Lindfors, A. Parssinen, and K. A. I. Halonen, "A 3-V 230-MHz CMOS Decimation Subsampler," IEEE Circuits and Systems II: Analog and Digital Signal Processing, vol. 50, pp. 105-117, Mar., 2003.

PLACE
PHOTO
HERE

Hyun Choi Biography text here.

PLACE
PHOTO
HERE

Alfred V. Gomes Biography text here.

PLACE
PHOTO
HERE

Abhijit Chatterjee Biography test here.